2007

Dynamically and Statistically Downscaled Seasonal Simulations of Maximum Surface Air Temperature Over the Southeastern United States

Young-Kwon Lim
Florida State University Tallahassee

D W. Shin
Florida State University Tallahassee

Steven Cocke
Florida State University Tallahassee

T E. LaRow
Florida State University Tallahassee

Justin T. Schoof
Southern Illinois University Carbondale, jschoof@siu.edu

See next page for additional authors

Journal Geophysical Research, 112, D24102, doi:10.1029/2007JD008764.

JOURNAL OF GEOPHYSICAL RESEARCH, VOL. 112, D24102, doi:10.1029/2007JD008764, 2007

Dynamically and statistically downscaled seasonal simulations of maximum surface air temperature over the southeastern United States

Young-Kwon Lim,[1] D. W. Shin,[1] Steven Cocke,[1] T. E. LaRow,[1] Justin T. Schoof,[2] James J. O'Brien,[1] and Eric P. Chassignet[1]

Received 9 April 2007; revised 27 June 2007; accepted 15 August 2007; published 21 December 2007.

[1] Coarsely resolved surface air temperature (2 m height) seasonal integrations from the Florida State University/Center for Ocean-Atmospheric Prediction Studies Global Spectral Model (FSU/COAPS GSM) (~1.8° lon.-lat. (T63)) for the period of 1994 to 2002 (March through September each year) are downscaled to a fine spatial scale of ~20 km. Dynamical and statistical downscaling methods are applied for the southeastern United States region, covering Florida, Georgia, and Alabama. Dynamical downscaling is conducted by running the FSU/COAPS Nested Regional Spectral Model (NRSM), which is nested into the domain of the FSU/COAPS GSM. We additionally present a new statistical downscaling method. The rationale for the statistical approach is that clearer separation of prominent climate signals (e.g., seasonal cycle, intraseasonal, or interannual oscillations) in observation and GSM, respectively, over the training period can facilitate the identification of the statistical relationship in climate variability between two data sets. Cyclostationary Empirical Orthogonal Function (CSEOF) analysis and multiple regressions are trained with those data sets to extract their statistical relationship, which eventually leads to better prediction of regional climate from the large-scale simulations. Downscaled temperatures are compared with the FSU/COAPS GSM fields and observations. Downscaled seasonal anomalies exhibit strong agreement with observations and a reduction in bias relative to the direct GSM simulations. Interannual temperature change is also reasonably simulated at local grid points. A series of evaluations including mean absolute errors, anomaly correlations, frequency of extreme events, and categorical predictability reveal that both downscaling techniques can be reliably used for numerous seasonal climate applications.

Citation: Lim, Y.-K., D. W. Shin, S. Cocke, T. E. LaRow, J. T. Schoof, J. J. O'Brien, and E. P. Chassignet (2007), Dynamically and statistically downscaled seasonal simulations of maximum surface air temperature over the southeastern United States, *J. Geophys. Res.*, *112*, D24102, doi:10.1029/2007JD008764.

1. Introduction

[2] Global general circulation models (GCMs) have often simulated large-scale climate scenarios with reasonable forecast skill. However, there still exists a recognizable gap between the current confidence level of GCMs' performance and the requirement for successful climate impact studies. In addition, recent studies have required the simulation of regional climate change scenarios with finer spatial and temporal resolution. Improved regional- to local-scale prediction is very important in that near-surface regional climate significantly determines consequences for many natural systems and human activities. Downscaling of GCM information to regional scale is, in this respect, an urgently requested research topic to provide people with better information on the regional climate.

[3] *Wilby and Wigley* [1997] and *Huth and Kysely* [2000] noted that downscaling techniques have emerged as a means of bridging the gap between what climate modelers are currently able to provide and what impact assessors require. Many downscaling techniques have been developed and applied to particular geographical areas such as European countries, South America, and western U.S. region [*Giorgi*, 1990; *Hewitson and Crane*, 1996; *Ji and Vernekar*, 1997; *Wilby and Wigley*, 1997; *Wilby et al.*, 1998; *Wilks*, 1999; *Fennessy and Shukla*, 2000; *Fuentes and Heimann*, 2000; *Huth and Kysely*, 2000; *Huth*, 2002; *Misra et al.*, 2003; *Widmann et al.*, 2003; *Robertson et al.*, 2004; *Feddersen and Andersen*, 2005; *Coulibaly et al.*, 2005; *Salathé*, 2005; *Sun et al.*, 2006]. Either a dynamical or statistical method has been applied for these downscaling studies. Several studies investigated building downscaling systems for operational use [*Juang and Kanamitsu*, 1994; *Hong and Leetma*, 1999].

[1] Center for Ocean-Atmospheric Prediction Studies (COAPS), Florida State University, Tallahassee, Florida, USA.
[2] Department of Geography and Environmental Resources, Southern Illinois University, Carbondale, Illinois, USA.

0148-0227/07/2007JD008764$09.00

[4] As the first attempt to construct this system over the southeastern United States region, covering Florida, Georgia, and Alabama, the Florida State University/Center for Ocean-Atmospheric Prediction Studies Global Spectral Model (hereafter referred to as GSM) has been downscaled to produce regional forecasts [*Cocke and LaRow*, 2000; *Shin et al.*, 2006; *Cocke et al.*, 2007]. This attempt is very important since (1) The individual local areas over the southeastern United States frequently face extremely high temperature and heavy rainfall with severe storms during summer, resulting in potential property damage and injuries; an accurate forecast, specifically for temperature and precipitation, with higher spatial resolution is essential to mitigate damage. (2) The southeastern United States is also noted for some of the largest areas of agricultural farms in the nation. Various kinds of crops and fruits (e.g., peach, tomato, corn, tangerine, peanut, citrus, and strawberry) are raised in these regions. Farmers and agricultural researchers need accurate climate forecasts to adapt management, increase profits, and reduce production risks. The present project therefore focuses on developing a downscaling system for surface temperature and precipitation and evaluating its performance in providing seasonal regional climate scenarios over the southeastern United States.

[5] There have been two types of downscaling techniques applied to the GCM simulations; dynamical and statistical methods. Dynamical downscaling is a method to nest a regional climate model into the domain of GCM. The regional model has a higher spatial resolution than the GCM and uses the GCM output for boundary conditions. The regional model is driven in a time-dependent mode by the global model at its boundaries. For this reason, the simulated regional climates are physically consistent with the GCM output. However, this also means that biases (see section 3.1.2) contained in the GCM can be passed to the regional climate model (RCM) [*Giorgi et al.*, 2001]. Several methods are developed for the sake of the reduction of those biases. In addition, previous regional model studies were limited to periods of only a few months [*Giorgi*, 1990; *Marinucci et al.*, 1995; *Rotach et al.*, 1997] or a few years because of the computational expense of the nesting method.

[6] Statistical downscaling encompasses a large number of methods, ranging in complexity from simple interpolations to eigentechniques, regression methods, stochastic time series models, and artificial neural networks [*Trigo and Palutikof*, 2001; *Reusch and Alley*, 2002; *Ramírez et al.*, 2006]. The most widely used statistical downscaling models are linear methods, such as local scaling, multiple linear regression, canonical correlation analysis, or singular value decomposition (SVD) [*Conway et al.*, 1996; *Schubert and Henderson-Sellers*, 1997; *Salathé*, 2003]. These methods are based on finding statistical relationships between sets of predictors and predictands. Usually, predictors can be chosen to be the large-scale dynamical model output whereas the predictands are the observed variables for the training period. During the training period important characteristics of regional climates are analyzed and then they are incorporated in the subsequent downscaling procedure, which facilitates the regionalization from the large-scale climate. Statistical downscaling also has an advantage over dynamical downscaling in that it can be carried out inexpensively. However, it is not clear which method provides better prediction of regionalized climate [*Xu*, 1999; *Schoof and Pryor*, 2001]. A limitation of statistical methods is that downscaled variables might not guarantee physical consistency between them since the complex physical processes including nonlinearity may not be fully considered in the method.

[7] We regionalized spring and summer surface temperature and precipitation for the southeastern United States using both dynamical and statistical downscaling methods. In this paper, we focus on discussing seasonal simulations of daily maximum temperature (T_{max}) over the southeastern United States, which is vulnerable to regional climate variability associated with extremely high temperature. Few dynamical or statistical downscaling methods have been applied to surface temperature of spring and summer for the southeastern United States. Simulations of downscaled precipitation, which are also very important for the southeastern United States, have been performed and we plan for their discussion in a subsequent manuscript.

[8] Dynamically downscaled temperatures are constructed from the FSU/COAPS Nested Regional Spectral Model (hereafter referred to as NRSM) [*Cocke and LaRow*, 2000; *Shin et al.*, 2006; *Cocke et al.*, 2007]. Model characteristics and experimental strategy are addressed in section 3.1. For statistical downscaling, a new technique has been developed primarily using Cyclostationary Empirical Orthogonal Function (CSEOF) [*Kim and North*, 1997] and multiple regression. CSEOF is used instead of conventional eigentechniques such as regular EOF and SVD because the spatial patterns of each mode extracted from CSEOF represent the complete spatiotemporal evolution of the important climate signals (e.g., seasonal cycle, prominent intraseasonal oscillations, and ENSO-related evolution) over a cyclic period [*Kim and Wu*, 1999]. The corresponding principal component (PC) time series represent the long-term amplitude fluctuation of these climate signals on an interannual timescale. CSEOF and the multiple regression method are trained with lower-mode PCs of the observation and the GSM to find out their statistical relationship. It is easier to use the CSEOF PC time series, which varies slowly with time, to determine the statistical relationship and corresponding regressed spatial patterns than other conventional PC time series, which often exhibit noisy high-frequency fluctuations. As a result, this approach facilitates the generation of the subsequent PC time series for the prediction period [*Lim and Kim*, 2006], resulting in the better localized climate scenario from the large-scale simulations.

[9] The remainder of this paper is organized as follows. The observational data and the global model output are described in section 2. Section 3 focuses on methodology and includes a description of the downscaling techniques and experimental design. The regionalized surface air temperatures are described in section 4, followed by discussion and concluding remarks in section 5.

2. Model Outputs and Observations

2.1. FSU/COAPS GSM

[10] The GSM provides the boundary conditions for the NRSM. The GSM is truncated at horizontal resolution of 63 waves (T63), which corresponds to approximately 1.875°

by 1.875° in the tropics, with 17 vertical levels within the sigma coordinate system. The GSM has a variety of physical parameterization schemes available to it, including the original FSU physics package and most of the National Center for Atmospheric Research Community Climate model (NCAR CCM) version 3.6 atmospheric physics package. For the configuration in this study, we use the NCAR CCM radiation and boundary layer physics. The model physics for the convective precipitation process is the simplified Arakawa-Schubert scheme [*Pan and Wu*, 1994]. Simulation of the land surface processes has recently been improved by including the NCAR community land model (CLM2) [*Bonan et al.*, 2002; *Shin et al.*, 2005] in the GSM. In this study, 7-month seasonal integrations for each year with the atmospheric initial conditions on 1 March are conducted for the period of 1994 to 2002. The initial conditions were provided by European Center for Medium-Range Weather Forecasts (ECMWF) analysis, which were available at T106 resolution, and the ocean information is given from prescribed SSTs, which are updated weekly. Output from the GSM run is used as a base input field for the NRSM. More details on the GSM including the model physics can be found in *Cocke and LaRow* [2000] and *Shin et al.* [2005].

2.2. Observed Surface Temperature

[11] The daily T_{max} data used in this study are from stations within the National Weather Service (NWS) Cooperative Observing Program. The Cooperative Observing Program has long history of more than 100 years to provide observational data required to define the climate of the United States and to help measure long-term climate changes. The program is the means by which the NWS obtains observational data to support both the climate program and its field operations (http://www.nws.noaa.gov/climate/). Cooperative Weather Stations, scattered over all 50 states, Puerto Rico, and the Virgin Islands, are taking weather observations 7 d a week throughout the year. The Cooperative weather observers provide a myriad of vital information for their local areas. The data set applied in this study is directly provided by the Florida Climate Center (http://www.coaps.fsu.edu/climate_center/) and covers the period of 1994 to 2002 with daily time interval. The station data obtained from 172 stations (Figure 1b) were objectively analyzed using the Cressman objective analysis scheme [*Cressman*, 1959] to 20 × 20 km grids over the domain. The resulting data set has approximately 1200 grid points with 20 km spatial resolution, covering states of Florida, Georgia, and Alabama. We compared both fields and confirmed that the gridded fields exhibit strong agreement with those from the station data. However, gridded fields over local areas where the distribution of stations is relatively sparse (e.g., southeastern Georgia, southwest Alabama, and southeastern tip of Florida) tend to be a little bit smoothed.

3. Downscaling Experiments

3.1. Dynamical Downscaling

3.1.1. FSU/COAPS Nested Regional Spectral Model (NRSM)

[12] The regional spectral model has been nested into the southeastern United States region of the GSM domain for the purpose of seasonal integration (Figure 1a). This regional spectral model, the NRSM, utilizes the base fields from the GSM. The base field is spectrally transformed to the regional grid and used for the boundary condition of the NRSM. In the NRSM, a 6-h nesting interval is used and the regional model uses the same physical parameterizations as the GSM. Nesting is currently one way, which means that regional solution is not fed back to the global model.

[13] The model uses a perturbation method similar to that used at NCEP [*Juang and Kanamitsu*, 1994] and ECMWF [*Hoyer*, 1987]. The NRSM predicts regional-scale perturbations to the GSM solution and the NRSM solution is the sum of the GSM solution and the perturbation field. The GSM is run first, and the prognostic base fields from the global model (wind, temperature, humidity, and surface pressures) are spectrally transformed, via a Fourier-Legendre transformation, from the global model output directly to the regional grid at a regular interval, every 6 h. The regional spectral perturbations from the previous time step or initial condition are then spectrally transformed via a double Fourier transform and added to the global values on the regional grid to obtain the full regional field. Once the full regional field is obtained, the physical and dynamical time tendencies are computed. Regional perturbation time tendencies are derived by subtracting the full regional model time tendencies from the global model time tendencies. The global model time tendencies are computed via a reverse semi-implicit algorithm of the transformed output, which have been linearly interpolated in time to the time step of the regional model. The regional perturbation time tendencies are then transformed to spectral space in order to solve the semi-implicit algorithm to obtain perturbations for the next time step. Details on the full description of the NRSM and its application to seasonal climate forecasting are found in *Cocke* [1998], *Cocke and LaRow* [2000], *Shin et al.* [2006], and *Cocke et al.* [2007].

[14] In this study, the NRSM was run at 20 × 20 km resolution. The 7-month integrations with the initial conditions provided by ECMWF analysis are performed, beginning on 1 March and ending on 30 September. These integrations are repeated for 9 years for the period of 1994 to 2002. This time period is exactly the same as that described for the GSM in section 2. Surface temperature variables including T_{max} and T_{min}, and several radiative flux variables are produced as a result of NRSM simulation. T_{max} exhibits greater variability during summer while daily T_{min} tends to be uniform throughout the season, which implies that skill evaluation for slightly oscillating T_{min} may not provide a meaningful assessment. This is specifically true for the southern part of the domain. We found that the region exhibiting substantial level of T_{min} variability is limited to northern Georgia and Alabama. Therefore we focus on addressing T_{max} fields in section 4. This presumption is equivalently applied to the statistical downscaling that will be introduced in section 3.2.

3.1.2. Bias Correction

[15] Reliability of the downscaling method depends on the accuracy of the GSM fields, as well as skillfulness of the method itself in regionalizing the GSM fields. Biases contained in the GSM fields will be carried to the NRSM scale during the nesting process. Therefore dynamically downscaled data should be bias corrected prior to evaluation.

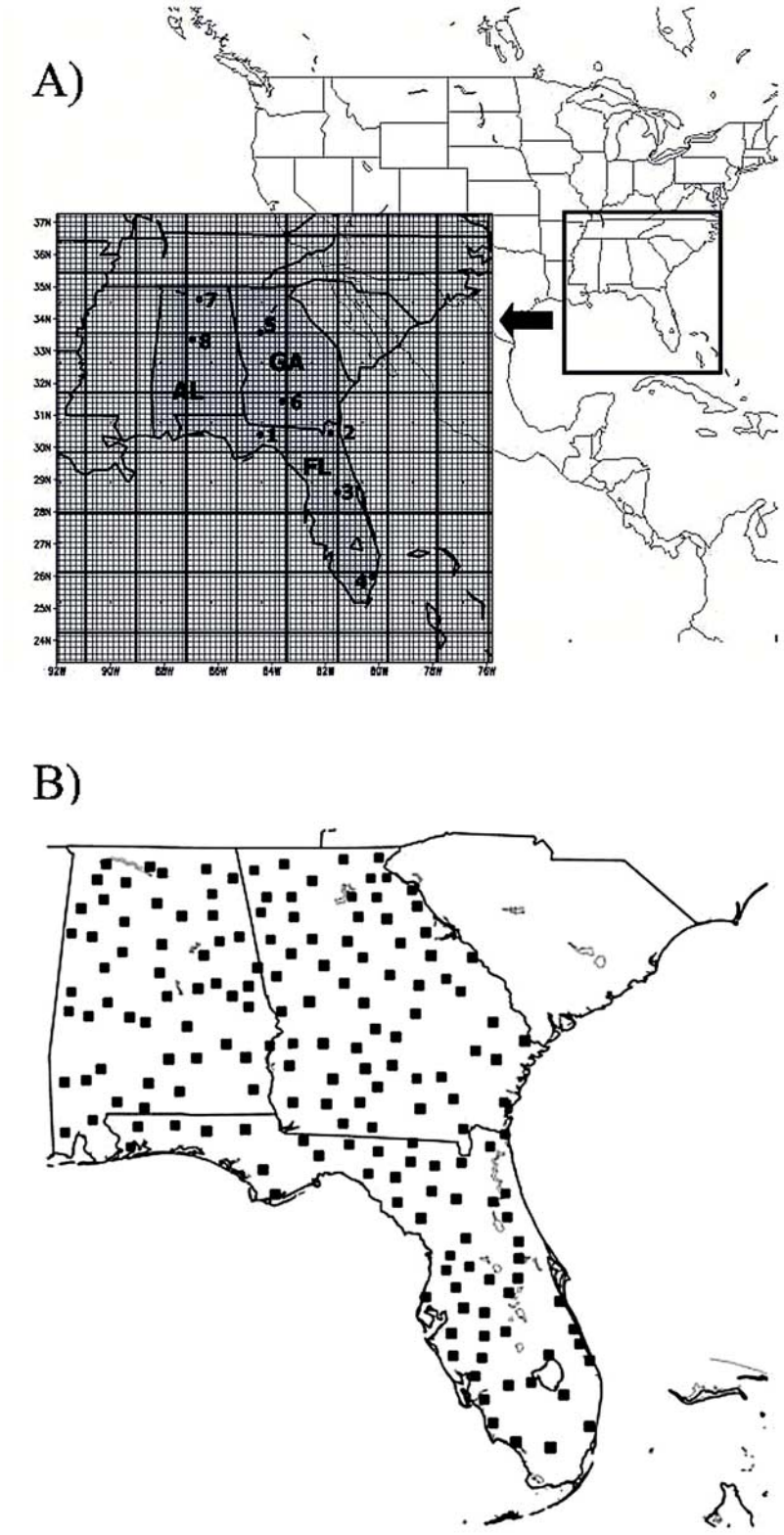

Figure 1. (a) Geographical areas of three states (FL: Florida, GA: Georgia, AL: Alabama) in the southeastern United States where the large-scale surface temperatures are regionalized by downscaling methods. Thick lines over the domain represent the spatial grids of the Global Spectral Model (GSM) whereas thin lines represent the local grid points applied in the Nested Regional Spectral Model (NRSM) and the statistical downscaling. Eight dots with numbers represent locations of cities, 1: Tallahassee, 2: Jacksonville, 3: Orlando, 4: Miami, 5: Atlanta, 6: Tifton, 7: Huntsville, and 8: Birmingham. (b) A map showing the station locations used for gridded observation data.

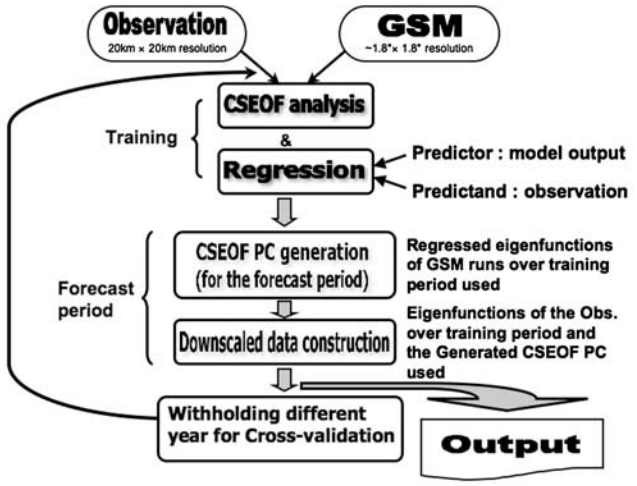

Figure 2. Schematic diagram of statistical downscaling procedure in the present study. Downscaling has been conducted using Cyclostationary Empirical Orthogonal Function (CSEOF), multiple regression, and the time series generation techniques. Downscaled data are produced over 9 years (1994–2002) by repeatedly withholding a particular year and placing it on the prediction period under the cross-validation framework.

[16] The bias correction employed here is described by *Wood et al.* [2002] and consists of remapping the exceedence probabilities (percentiles) of the simulated data to those of the observed data. We replace the daily NRSM simulated values with values having the same percentiles as from observations. To this end, we estimate the probability distribution for each month using daily NRSM values and observations, respectively. The number of values used for estimating the probability distribution for March, for example, is 279 (=31 d × 9 years). Suppose that we have a downscaled value of T_{max} (say 30°C) at the 60th percentile of the downscaled T_{max} probability distribution (that is, not to be exceeded more than 40% of the time). Then, the associated T_{max} having the same exceedence probability in the observed distribution is calculated. Finally, we replace the downscaled T_{max} value (30°C) with the associated T_{max} obtained by the previous step. This bias-corrected value will be the 60th percentile of the observed T_{max} probability distribution. The above steps are repeated for other daily downscaled T_{max} values. Bias correction is performed at the NRSM scale by treating each NRSM grid cell, defining its own temperature distribution. Each month is treated independently in this bias correction so that seasonal variations in bias can be accounted for. Therefore underlying biases are not identical over the 7 months.

[17] The conventional bias correction method by removing the climatological mean assumes that there is only a bias in the mean. The bias correction in this study accounts for bias in higher moments as well.

3.2. Statistical Downscaling

[18] The techniques primarily applied in this study are Cyclostationary EOF (CSEOF) [*Kim and North*, 1997] analysis, multiple regression, and the stochastic time series generation. The downscaling procedure is illustrated schematically in Figure 2. CSEOF analysis is one of many eigentechniques used to decompose the data into a set of independent modes and their PC time series. The major difference between CSEOF analysis and other eigentechniques is that the spatial patterns of each mode extracted from CSEOF represent the complete spatiotemporal evolution of the prominent climate signals (e.g., seasonal cycle, prominent intraseasonal oscillation, and ENSO-related evolution, etc.) over a cyclic period. The corresponding PC time series represents the long-term amplitude fluctuation of this climate signal on an interannual timescale. Therefore space-time data in CSEOF analysis are represented as

$$P(r,t) = \sum\nolimits_n S_n(t) B_n(r,t) \tag{1}$$

where $B_n(r, t)$ are time-dependent cyclostationary loading vectors and $S_n(t)$ are their PC time series. The main purpose of applying CSEOF analysis is to extract the spatiotemporal evolution of climate signals and their long-term amplitude variations from both observation and GSM output for the training period. Therefore CSEOF analysis, as the first step of this downscaling, is applied to the daily observation and the GSM output, respectively, for the first 8-year training period. The remaining ninth year is regarded as the prediction period which we perform the regionalized simulation on the basis of the identified statistical relationship. The spatial domain for applying CSEOF analysis to the GSM output is 100°W–65°W and 16°N–38°N, which is large enough to recognize the large-scale characteristic patterns encompassing the southeastern United States.

[19] An example of CSEOF spatial patterns from both observation (left two columns) and GSM output (right two columns) is presented in Figure 3. Since CSEOF is applied to the daily data, CSEOF modes are produced at daily time steps over a cyclic period. In Figure 3, we took the temporal average of the 1st CSEOF modal patterns over ~15 d and show them for spring season (March, April, and May). While the left two columns represent the CSEOF patterns for observation, the right two columns for the GSM represent CSEOF patterns obtained by regression onto the 1st mode of observation. We describe in the next paragraph how to construct these patterns via multiple regression. Regressed patterns show how the GSM anomalies having warm or cold biases are linked with the observed 1st CSEOF patterns. On the basis of this relationship, the downscaling procedure can correct warm or cold biases contained in the GSM output. Figure 4 shows an example of a CSEOF PC time series for the first two observed and simulated modes. They are at daily time steps but they vary slowly on an interannual timescale. Those PC time series are used for multiple regression, which is the next downscaling step (Figure 2).

[20] The multiple regression is performed for the purpose of finding out the statistical relationship between the prominent climate signals of observation and the GSM. Multiple regression is applied to the extracted climate signals and the corresponding PC time series obtained from both observation and the GSM output. To find physically and dynamically consistent modes, the observed CSEOF mode is declared as a target variable followed by regression of the

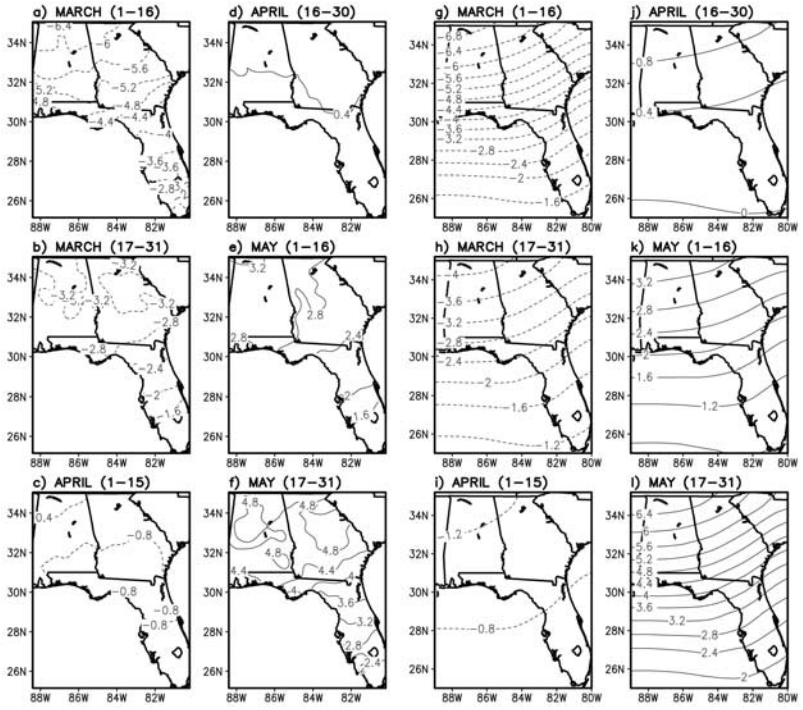

Figure 3. Left two columns (a–f): The 1st mode CSEOF patterns for observation. Right two columns (g–l): CSEOF patterns for the GSM which are obtained by regression onto the first observed CSEOF mode. CSEOF patterns originally at daily time step have been taken average over ~15 d, and resulting patterns are shown for spring season (March, April, and May).

model CSEOF mode (predictor) onto the target variable. For this regression, the PC time series of the first 10 modes of a predictor variable, which explain approximately 99% of the total variance, are regressed onto a certain PC time series of the target variable (observed CSEOF) by multiple regression. That is,

$$PCT_n(t) = \sum\nolimits_i \alpha_{ni} \cdot PCP_i(t) + \varepsilon(t), \quad i = 1, 2, \cdots, 9, 10 \quad (2)$$

where $PCT_n(t)$ are the nth mode target PC time series, α_{ni} are the regression coefficients, and $PCP_i(t)$ are the predictor PC time series. Regression coefficients are determined such that the variance of regression error, $\varepsilon(t)$, is minimized. Once regression coefficients are computed, they represent weights for each mode (i = 1, ···, 10) of predictor eigenfunctions to construct the regressed large-scale patterns, which are physically consistent with the nth mode of predictand eigenfunctions.

[21] On the basis of the statistical relationship between the climate signals of observations and the GSM outputs, CSEOF PC time series are generated for the prediction period (Figure 2). The equation for the PC time series generation is given as

$$PC_n(t) = \sum\nolimits_g P(g,t) \cdot B_n^+(g,t), \quad (3)$$

where $PC_n(t)$ are the nth mode PC time series for the prediction period, B_n^+ (g, t) are the regressed CSEOF eigenfunctions for the nth mode, g is the large-scale grid point, and $P(g, t)$ are the GSM anomaly over the prediction period. In this study, $PC_n(t)$ is estimated by a windowed spectral analysis [*Ogura*, 1971]. Thus smoothness of $PC_n(t)$ may depend on the width of spectral window.

[22] The subsequent procedure is to construct the downscaled data for the prediction period using the generated PC time series and the eigenfunctions identified from training (Figure 2). The downscaled data are finally constructed by

$$D(s,t) = \sum\nolimits_n PC_n(t) \cdot B_n^o(s,t), \quad (4)$$

where PC_n (t) are the generated PC time series obtained from equation (3), $B_n^o(s, t)$ are the CSEOF eigenfunctions of the observation obtained from training, and $D(s, t)$ are the

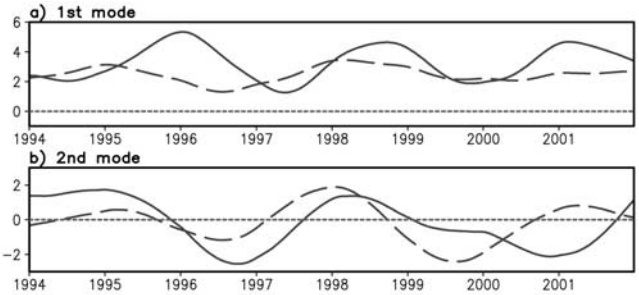

Figure 4. Example of CSEOF principal component (PC) time series for the first two observed (solid line) and GSM simulated (long-dashed line) mode. In this example, 8 years from 1994 through 2001, which is the training period, is used for CSEOF analysis.

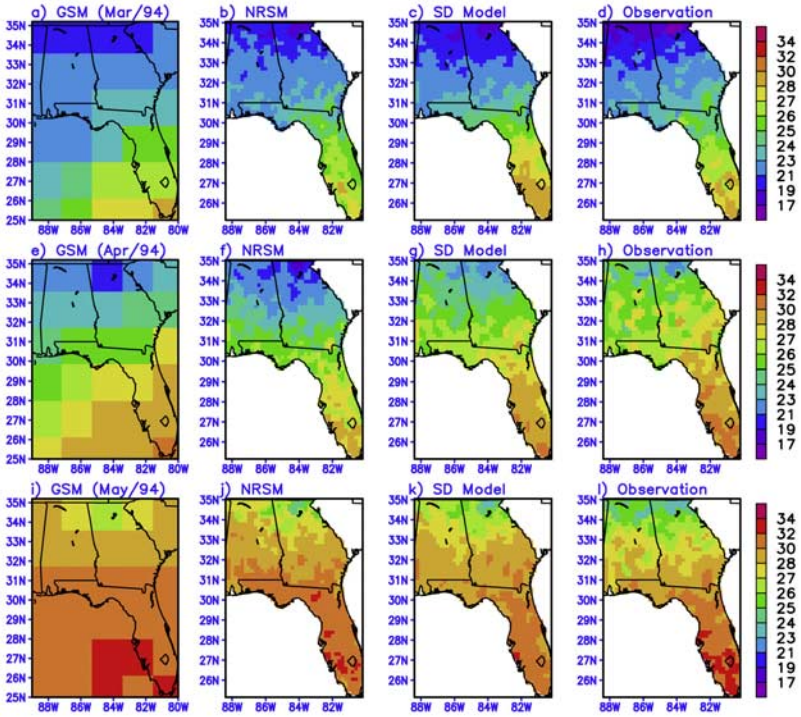

Figure 5. Geographical distribution of monthly averaged surface T_{max} for spring in 1994. Each column from the left indicates the monthly mean field derived from (1) the GSM (a, e, i), (2) dynamical downscaling (the NRSM) (b, f, j), (3) statistical downscaling model (c, g, k), and (4) observation (d, h, l).

downscaled temperatures at regional grid point *s* over the prediction period.

[23] The procedure delineated above is repeated by withholding a particular year and put it in the prediction period for the sake of cross validation. As a result, downscaled daily T_{max} fields for the entire 9 years (1994–2002) are constructed.

4. Seasonal Simulations of Downscaled T_{max}

4.1. Monthly Mean Field

[24] Downscaled daily T_{max} are averaged over each month to construct the monthly means and they are compared with observation and the bias-corrected GSM fields. Evolution of monthly mean fields during 1994 is shown in Figures 5 and 6 as example to illustrate how the downscaled fields better regionalize detail than the GSM fields in simulating the regional climates.

[25] Figures 5 and 6 indicate that large-scale spatial patterns at a glance from downscaled models (the second and third columns), observations (the fourth column), and the GSM (the first column) are not much different from one another at contemporaneous periods. Both downscaling models and the GSM successfully reproduce the seasonal progression of T_{max} from March through August. However, as seen in the left three columns, spatial temperature differences at the regional scale are much better realized in the downscaled data, while those differences are not reasonably captured in the GSM. For instance, (1) Spatial patterns over the northern part of the domain (northern Georgia and Alabama) exhibit more similarity to observations from the two downscaled models than from the GSM fields. (2) Complicated local structures over the middle part of the domain (southern Georgia and Alabama, and northern Florida) found from observations tend to be better reproduced by the downscaled fields. (3) Regional differences over central and southern Florida tend to be better realized by downscaling, while the GSM fields tend to be uniform over that area. (4) Biases appear to be smaller in downscaled fields than in the GSM fields, as they show larger overestimate of the July and August mean (Figure 6). The northern part of the domain is also overestimated by the GSM starting in May (Figures 5 and 6).

[26] As stated in the previous paragraph, overall patterns from the present downscaling models reasonably predict the regional surface T_{max} over the southeastern United States. Simulation of the regional distribution for the remaining 8 years, which are not individually shown here, is reasonable as well. The GSM fields exhibit reasonable capability of producing the distribution of surface T_{max}, but lack the spatial resolution to provide fine-scale information.

4.2. Seasonal Variation and Mean Absolute Error

[27] The seasonal variation of the downscaled data is examined, along with its comparison with the observations. Figure 7 shows the time series on a monthly timescale for eight selected local grid points over the entire 9 years. Four cities (Tallahassee, Orlando, Jacksonville, and Miami) are selected in Florida, and two cities are respectively selected in Georgia (Atlanta and Tifton) and Alabama (Huntsville and Birmingham) such that those grids are evenly distributed over the southeastern United States domain (Figure 1a). The time series are plotted with observations (black). The most notable feature in Figure 7 is that the seasonal

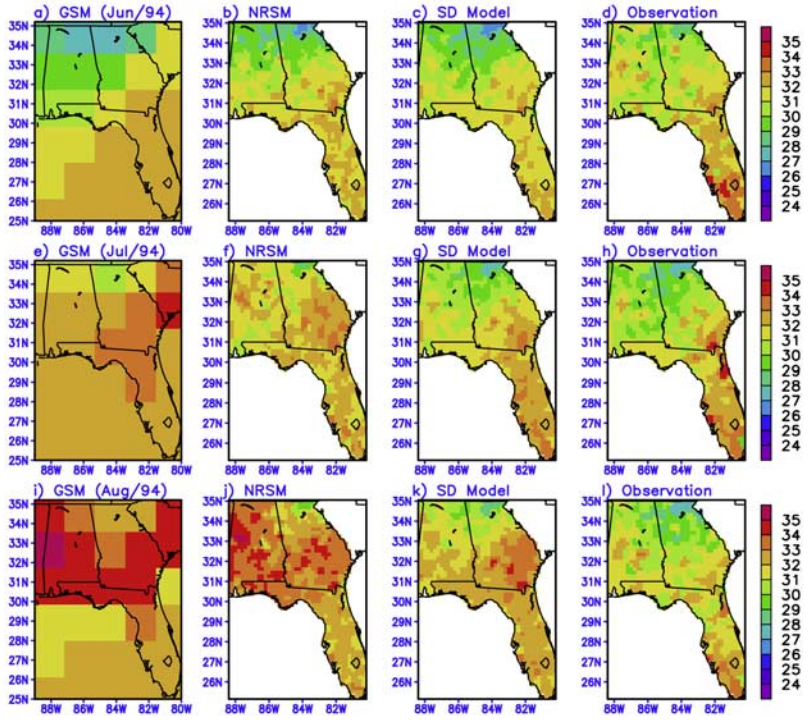

Figure 6. Same as Figure 5 but for summer 1994.

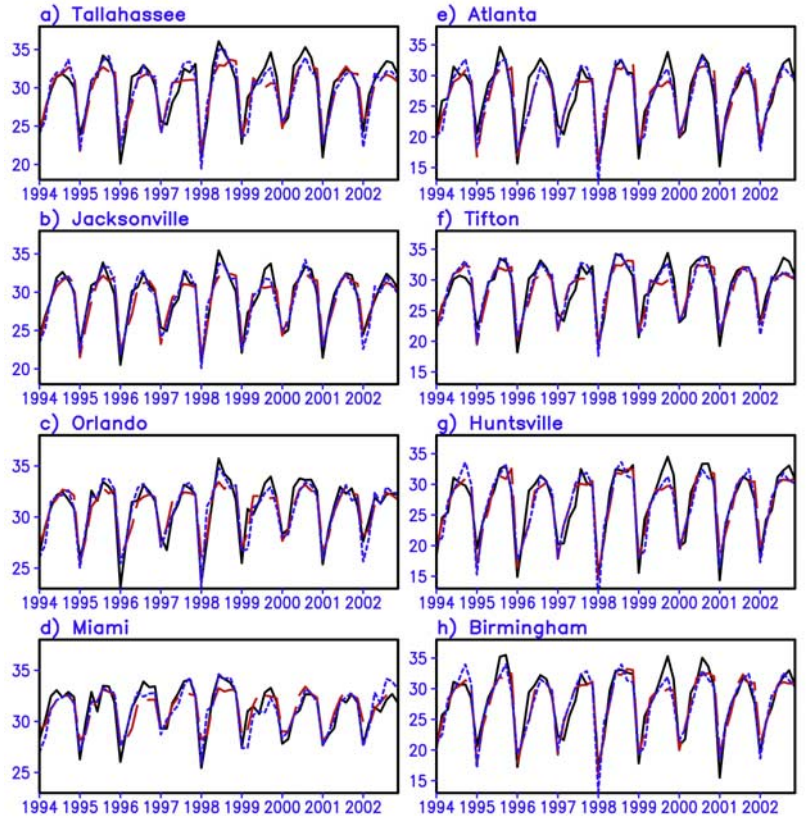

Figure 7. Monthly averaged surface T_{max} time series for the selected eight local grid points over 9 years (1994–2002) obtained from (1) statistical downscaling (red), (2) dynamical downscaling (the NRSM) (blue), and (3) observation (black). Monthly mean starts from March through September for each year. Abscissa denotes the year, whereas the ordinate denotes the temperature in Celsius.

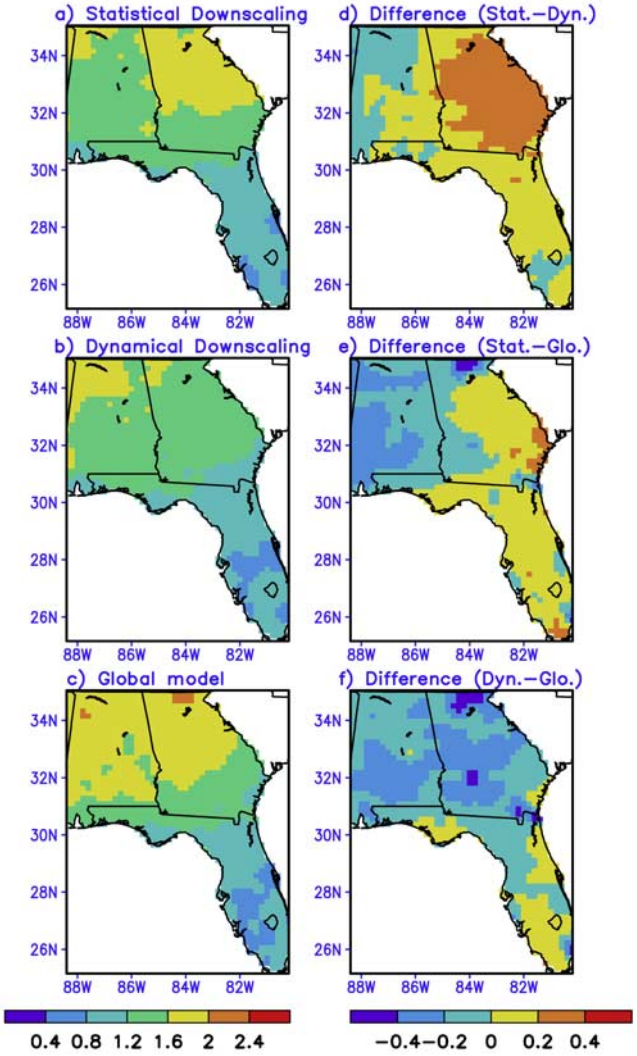

Figure 8. Mean absolute error maps for the monthly averaged surface temperatures downscaled from the GSM (a and b). Errors are obtained by averaging the absolute value of difference between observation and downscaled data each month over 9 years considering March through September at each local grid points. (left) Errors for statistical downscaling (top), dynamical downscaling (the NRSM) (middle), and the regridded GSM (bottom). (right) Differences in their errors. Color scale is denoted by color bar attached on the bottom of each column.

variations seen in the observation are successfully reproduced by each downscaling method, plotted by red and blue curves, at the local grid points. Biases of the GSM fields, which were carried to the NRSM, have been corrected by the method described in section 3.1.2 [*Wood et al.*, 2002].

[28] For the statistical downscaling, on the other hand, the GSM biases are implicitly corrected in the process of downscaling. For example, the GSM time series unveil cold biases over southern Florida including Orlando and Miami (not shown here) since the GSM grid boxes over that area partly cover the ocean as well (see Figure 1a). These cold biases over inland southern Florida are corrected by the statistical downscaling. The GSM biases found in other regions were also significantly reduced by the statistical downscaling and as a result, the statistically downscaled time series exhibit seasonal variation much closer to observation. However, the statistically downscaled time series sometimes underestimate the summer temperature at the selected local grid points (Figure 7), while the NRSM underestimates very little the observed monthly mean for summer. One of the characteristics of statistical downscaling is that it occasionally underestimates the observed amplitude and variability [*Schmidli et al.*, 2007].

[29] Mean absolute errors of these downscaled time series with respect to the observed time series are shown in Figure 8. The errors are obtained by averaging the absolute value of difference between observation and downscaled data each month over 9 years for March through September at each grid point. For comparison with the downscaled results, error fields for the GSM output, which has been regridded by an objective analysis [*Cressman*, 1959], are also plotted in Figure 8c. The key feature is that the absolute magnitude of the error ranges from 0.4° to 2.0°C, which can be considered reasonable for the fine spatial scale (20 km) of monthly surface temperatures [*Murphy*, 1999; *Zhu and Liang*, 2007]. These spatial error patterns are found alike for both downscaling methods, as seen in Figures 8a and 8b. Previous downscaling studies for other geographical areas have shown error magnitudes comparable to or slightly larger than those computed in this study [*Nicolini et al.*, 2002; *Oshima et al.*, 2002; *Boé et al.*, 2006]. These studies also reported that the error magnitude in summer T_{max} tends to be larger than that in winter, indicating that the correct simulating of T_{max} is more challenging in summer.

[30] Comparison in mean absolute errors between downscaled and direct GSM data shows that averaged over the domain, the NRSM simulations exhibit smaller errors than the GSM or statistically downscaled simulations (Figures 8d and 8f). Only the western half of Alabama and part of southeastern Florida exhibit the smallest error by statistical downscaling and the regridded GSM, respectively (Figures 8d–8f). Either downscaling method reveals smaller errors than the GSM over most grid points. However, part of southeastern Florida, where temporal amplitude variation is smaller than northern areas, happens to exhibit smaller error by the objectively analyzed GSM. Our calculation using the observed monthly temperature reveals that southern Florida has the smallest standard deviation, which is about two thirds as big as that over Alabama and Georgia (not shown). Regional comparison in distribution of errors shows that Florida has smaller errors than the other two states (Figures 8a–8c). This could also result from smaller temporal variability in this region, not necessarily from the greater predictive skill than the other states.

4.3. Anomalies and Correlations

[31] Downscaled T_{max} have been averaged to obtain seasonal means for spring (MAM) and summer (JJA) seasons. Seasonal anomalies are then obtained by subtracting the average values for the season, averaged from 1994 through 2002. Seasonal means and anomalies are investigated, along with correlations for the monthly and seasonal anomaly fields. Figure 9 shows the seasonal mean fields for

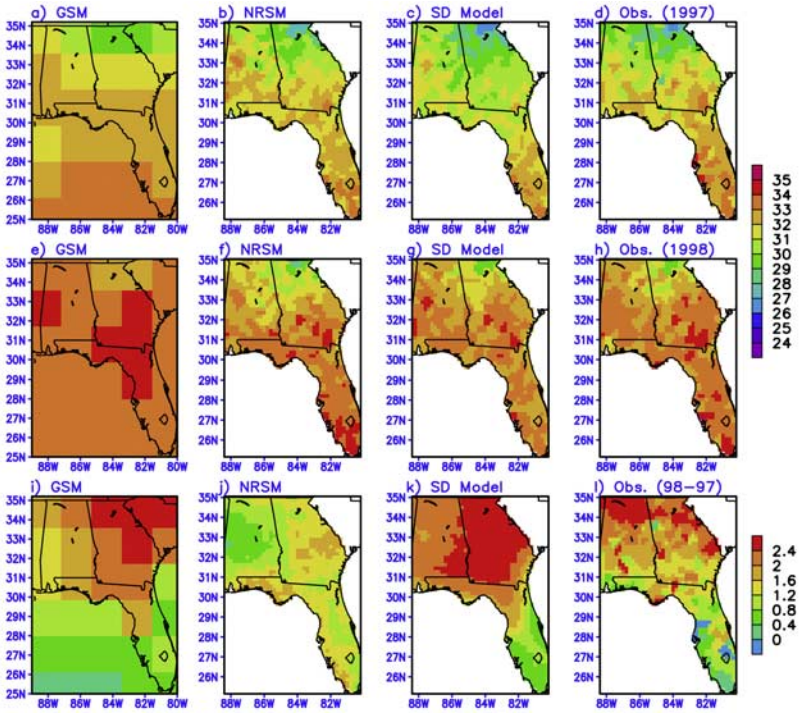

Figure 9. Geographical distribution of seasonally averaged surface T_{max} for summer in 1997 (top), 1998 (middle), and their difference (98 − 97) (bottom). Each column from the left indicates the fields derived from (1) the GSM (a, e, i), (2) dynamical downscaling (the NRSM) (b, f, j), (3) statistical downscaling (c, g, k), and (4) observation (d, h, l).

summer in 1997 and 1998 as examples, when one of the strongest ENSO events was recorded. The ENSO warm event reached maturity in winter of 1997 and abruptly decayed May 1998 [*Takayabu et al.*, 1999]. Figure 9 shows the interannual temperature difference between the 2 years (Figure 9, bottom). Higher (lower) temperature in 1998 (1997) with detailed spatial structure is faithfully simulated by the two downscaling methods (Figures 9b–9c and 9f–9g). These downscaled fields better exhibit detailed temperature patterns at smaller scales (Figures 9b–9d and 9f–9h) than the GSM fields shown in Figure 9, left (Figures 9a and 9e). It is obvious that the GSM fields have limited capability to realize the regional temperature fields over the domain.

[32] Figure 10 shows the seasonal anomaly time series for eight selected local grid points over 9 years. The time series are plotted with the observations (black solid). It is apparent that temporal peaks identified from the observation are faithfully captured by downscaled T_{max} time series, denoted by red and blue solid lines (Figure 10). The warm seasonal anomaly in 1998 summer, when the strong ENSO event with abnormal surface temperatures and rainfall were recorded [*Changnon*, 1999], for instance, is successfully reproduced by the downscaled time series. We can also find the downscaled peaks coinciding with the observed ones at many other periods. Those peaks are often closer to observation than peaks of the GSM time series (dashed curves), although there are some exceptions in some time periods. Overall, the anomalies simulated by both downscaling methods appear to correlate well with the observation.

[33] Both downscaling methods appear to have the comparable skill in capturing the observed temporal fluctuations. Not all periods at every local grid, however, captures these observed fluctuations accurately. Spring of 1995 is an example when the downscaled time series behave oppositely to the observed time series (black curves). This behavior is also seen in Alabama in summer of 1999 (Figures 10g and 10h). Tendency of temporal fluctuation in 1997 spring has not been properly captured over locations except Miami and Jacksonville. The relatively poor downscaling at these periods arises from poor simulation of the GSM temperature anomaly at these periods (see dashed curves) since the skill of downscaling tends to depend on the performance of parent global model to a certain extent.

[34] Temporal correlation coefficients are calculated for the downscaled seasonal anomalies shown in Figure 10. Correlation maps in Figure 11 reveal that the correlations for the seasonal anomaly of T_{max} exceed 0.3 over all local grid points except northwestern Alabama and a few grid points over southwestern Florida (Figures 11a and 11b). Most locations in Florida, southern Alabama and southwestern Georgia from the statistical downscaling have correlation from 0.5 up to 0.8 (Figure 11a). Correlations for the dynamically downscaled T_{max} are higher than those for statistical downscaling over Georgia and part of eastern Florida, as shown in Figures 11b and 11c. Many local grid points over the middle of the southeastern United States domain show correlations greater than 0.5 and some areas reach 0.8. Areas where the statistical downscaling exhibits much better performance are Alabama and southern Florida (Figure 11c).

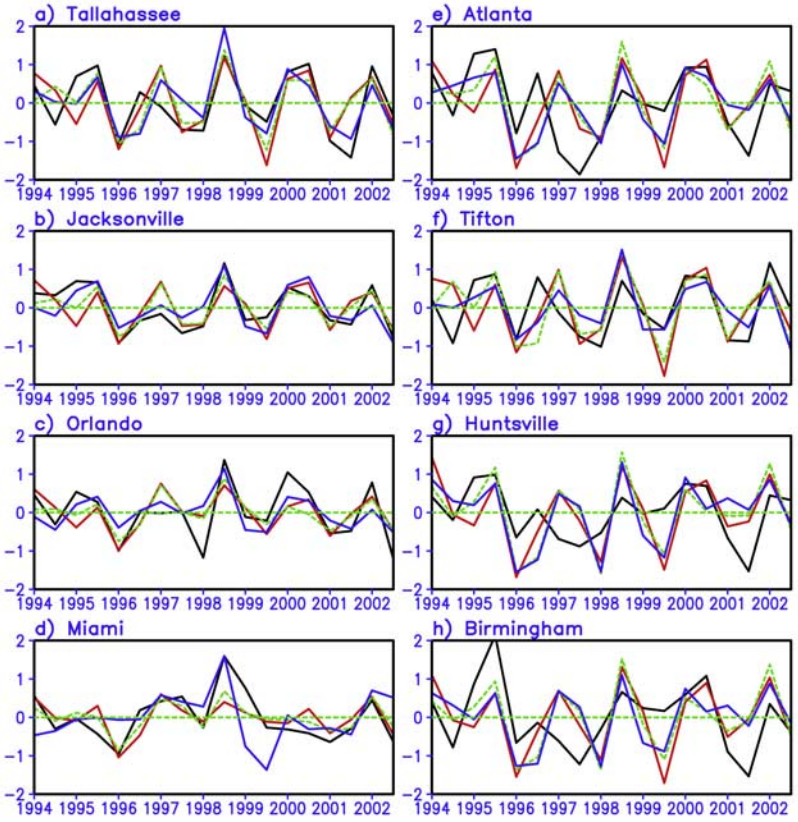

Figure 10. Downscaled time series of the seasonal T_{max} anomalies for the selected eight local grid points over 9 years. Downscaled daily temperatures have been averaged over spring (MAM) and summer (JJA) season, respectively, to construct the seasonal mean T_{max}. Seasonal anomalies are then obtained by subtracting the average values for that season, averaged from 1994 through 2002. Time series obtained from (1) statistical downscaling, (2) dynamical downscaling (the NRSM), (3) observation, and (4) the GSM are, respectively, plotted by red solid, blue solid, black solid, and dashed curves.

[35] The overall spatial pattern of correlations for monthly anomaly, depicted in Figure 11, right, is not much different from patterns for seasonal anomaly. For example, Florida and southern part of Georgia and Alabama show relatively higher correlation than other regions, while northwestern Alabama shows the lowest correlation from the dynamical downscaling. Correlation values at nearly all grids, however, have been reduced compared with correlations for seasonal anomaly. Correlations range from 0.1 to 0.5 and most of low correlations are found over northwestern Alabama and northern Georgia, from both downscalings (Figures 11d and 11e). One possible reason for the poorer skill in the inland regions may be due to the inability of the GSM to capture the proper climate signals in these regions as discussed by *Cocke et al.* [2007]. That study shows that the coastal region has higher predictability of large-scale climate than the inland region in winter. It is possible, but rigorous examination remains to be shown that this predictability can be extended to spring or summer. Our calculation of correlation between regridded GSM and observation for spring and summer also produced the lowest-correlation values over western Alabama.

[36] Figure 11, bottom, depicts the comparison in correlations between the two downscaling methods for seasonal (Figure 11c) and monthly anomalies (Figure 11f). Correlations from statistical downscaling are slightly higher over Alabama, northern and southern Florida, and western border of Georgia. The remaining areas show higher correlation from dynamical downscaling. However, the difference in these correlations is generally less than 0.1, indicating either of these two downscaling methods is not significantly better than the other. These results are similar to those obtained in other comparisons [*Díez et al.*, 2005].

4.4. Frequency of the Extreme Daily Temperature Events

[37] Surface temperatures that are much warmer or cooler than normal may provide unfavorable conditions for regional agriculture, water cycle, and human comfort and even human mortality. For instance, extended periods of hot weather over the southeastern United States during summer may give unfavorable conditions for regional agricultural production. We now investigate the number of daily T_{max} events which exceed 1 standard deviation above the daily climatological mean, for each season. Variation of the number of these events is plotted for spring and summer for the eight local grid points in Figure 12.

[38] In the discussion that follows, 1 standard deviation above the climatological mean as the threshold to define an extreme daily event is obtained from the respective downscaling method. Since the variance of T_{max} is not the same for each downscaled method, the threshold for an extreme

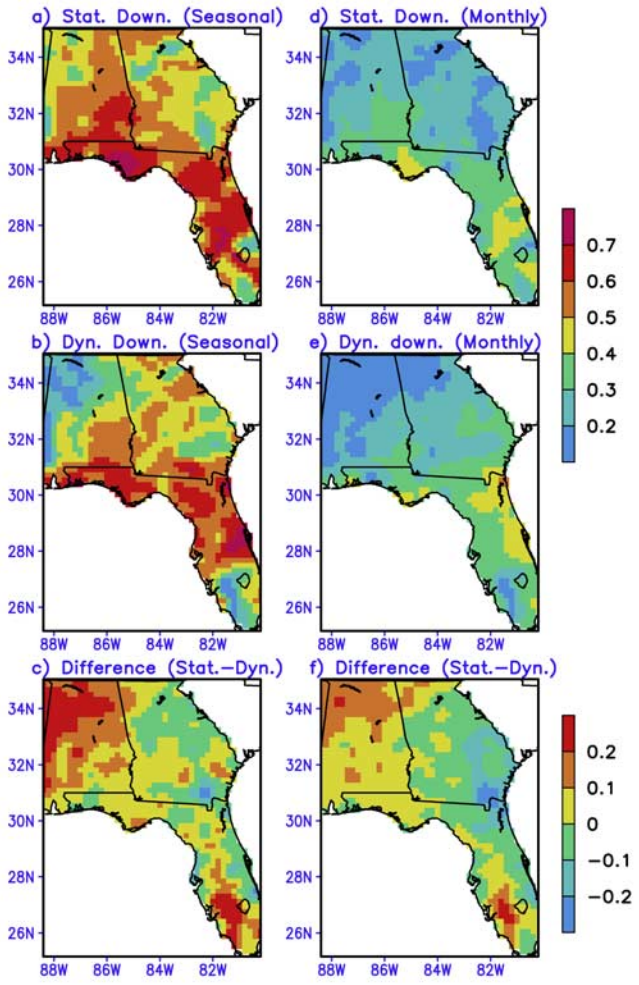

Figure 11. Correlation maps for the downscaled temperature anomalies over 9 years and two seasons (spring and summer). Climatology has been removed from the data before calculating correlations. (left) Correlations for the seasonal T_{max} anomaly. (right) Monthly T_{max} anomaly. Correlation of statistical downscaling (top), dynamical downscaling (the NRSM) (middle), and their differences (statistical−dynamical) (bottom). Color scale is denoted by color bar attached on the right side.

event will differ. The bias correction method used for dynamical downscaling ensures that the modeled variance is close to observations. For the statistical approach used here, as with most statistical methods, the variance tends to be lower than observed, thus necessitating using a lower threshold to define an extreme event.

[39] The time series for extreme T_{max} occurrence depicts that the time series obtained from the downscalings are quite consistent with the observed time series. For example, the season when the greatest number of extreme daily T_{max} events was recorded is 1998 summer (Figure 12). During that season, especially for June, more frequent fires occurred in Florida than other periods [*Changnon*, 1999]. This abnormal number of warmer T_{max} events is observed at all eight grid points with higher amplitude than any other time period. Downscaled T_{max} successfully simulates these frequent warmer T_{max} events during this season, as plotted by dashed and long-dashed curves.

[40] Each grid point shows somewhat different features for the seasonal variation in the extreme T_{max} frequency. For instance, observation in Miami, denoted by solid curves, shows larger T_{max} frequency value in 1997 summer than any of the other seven grid points. Those grid points, on the other hand, experience frequent extreme T_{max} events in 2000 summer and 2002 spring whereas the signal in Miami is not significant. Birmingham and Atlanta exhibit remarkably the more frequent extreme T_{max} events in 1995 summer than the other grid points. Notable features including those referred to above are fairly well simulated by both downscaling methods (dashed and long-dashed curves). Correlation coefficients in Figure 13, right, also support that both downscaling methods reasonably simulate the variation of frequency of extreme T_{max} events (corr. > 0.4) except for northern Georgia and Alabama, and southwestern tip of Florida.

[41] However, time series in Figure 12 also indicates that there is also room for improvement of these downscaling techniques. The statistical downscaling overestimates the extreme T_{max} frequency in Miami during 2000 summer and 2002 spring, while the dynamically downscaled data underestimate the frequency in 2000 summer for Tallahassee, Orlando, Huntsville, and Birmingham. The frequency in 1997 spring tends to be overestimated by statistical downscaling whereas the value in 1999 summer is not properly captured by both downscaling methods. Figure 13, left, illustrates that mean absolute difference in the number of daily extreme events by season primarily lies in the range of 6 to 10 from dynamical downscaling (Figure 13b), while the statistical downscaling shows greater difference up to 12. The average number of the events by season from observation is more or less than 15 over the domain (not shown), indicating that problems with significant overestimation/underestimation should be improved specifically in the statistical downscaling method.

4.5. Categorical Forecast for the Above/Below Climatological Average

[42] Categorical predictability for the above/below climatological seasonal average is evaluated at individual local grid points. Seasonal surface T_{max} anomalies are classified into two cases, above or below climatological average. The same sign of seasonal anomalies between observation and downscaled ones indicates a correct categorical forecast of the surface T_{max} anomaly. Figures 14a (statistical downscaling) and 14e (dynamical downscaling) depict the geographical distribution of the percentage correct ($(P_{aa} + P_{bb}) \times 100$, see Table 1) for simulating the above/below climatological T_{max} average at each local grid. Results illustrate the percentage correct ranging from 60% to 80% by both downscaling methods, indicating that our downscaling methods yield perceptibly greater predictability than random chance. Only a few grid points show a percentage correct between 50 and 60. The percentage correct between 60 and 80 over most grid points is encouraging as the southeastern United States is a more challenging region to achieve reasonable predictive skill than any other region in the United States in summer [*Saha et al.*, 2006]. Although direct comparison is limited because *Saha et al.* [2006]

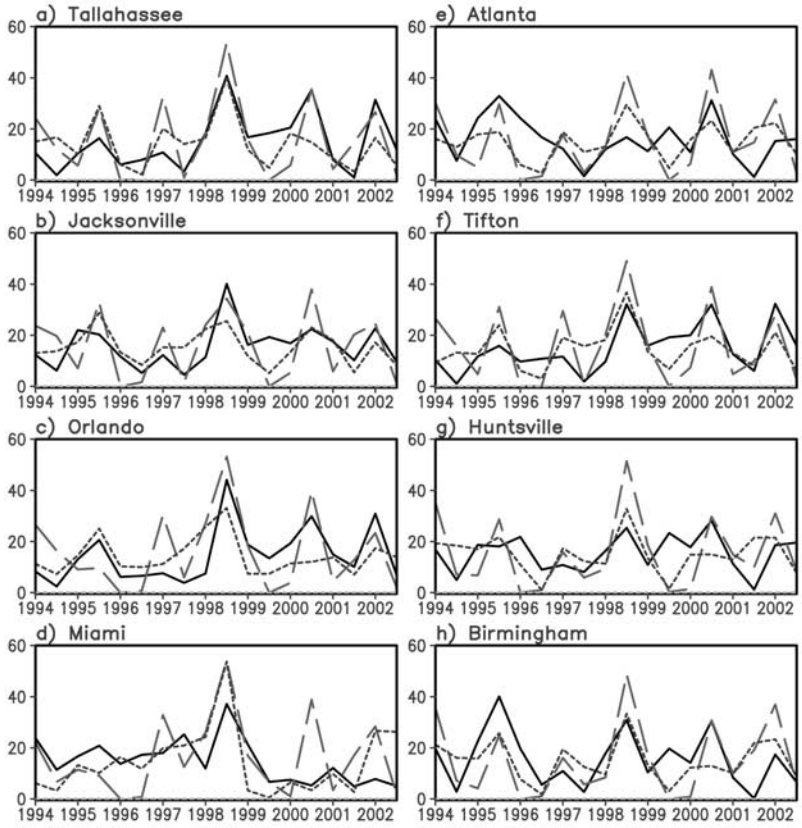

Figure 12. Variation of the number of extreme daily T_{max} events for each season at the selected local grid points. Events in which the daily T_{max} anomaly exceeds the 1 standard deviation plus climatology are counted each season. Time series from (1) statistical downscaling, (2) dynamical downscaling (the NRSM), and (3) observation are, respectively, plotted by long-dashed, dashed, and solid curves. Abscissa denotes time (two seasons per year), whereas the ordinate denotes the number of extreme daily T_{max} events for each season.

deals with the seasonally forecasted (i.e., forecast SSTs are used) large-scale surface mean temperature, the NCEP climate forecast system reported that skill for the seasonal surface air temperature is restricted to the northwest United States while most of the country including the southeastern United States has no demonstrable skill.

[43] Comparison in predictive skill between two downscaling methods reveals that categorical seasonal anomaly in Alabama is better regionalized by statistical downscaling, while the dynamical method is better than statistical one in Georgia (Figures 14a and 14e), the same feature as seen from the correlation fields (Figure 11c). Skill in Florida is not significantly distinguished by either of these two downscaling methods.

[44] The rightmost columns of Figure 14 show the Heidke skill score (HSS) [*Heidke*, 1926; *Jolliffe and Stephenson*, 2003] calculated on the basis of the categorical correctness in regionalizing the above/below climatological seasonal average. The HSS is a commonly used categorical verification score, measuring categorical matches between simulations and observations [*Barnston*, 1992]. The basic equation for the HSS is given as

$$HSS = \frac{P_C - P_E}{1 - P_E} \tag{5}$$

where P_C and $P_E = P_a^P\ P_a^F + P_b^P\ P_b^F$ (see Table 1) are probabilities of a correct forecast and a random forecast, respectively.

[45] Figure 14d shows that HSS values for the statistically downscaled T_{max} are positive for all but a few grid points over Florida and northeast Georgia. Alabama and the northwestern Florida show the highest HSS, with scores greater than 0.4, while northeast Georgia and southernmost Florida, which correlates relatively low (corr. $\approx$ 0.3) with the observed T_{max} (Figure 11a), show negative HSS. HSS values over the remaining grid points are positive, mostly ranging from 0.2 to 0.5. Figures 14b and 14c further support that the ratio for incorrect forecast is much lower than the percentage correct shown in Figure 14a. The formula applied for the calculation of Figures 14b and 14c is, $\frac{P_{ab}}{P_{aa}+P_{ab}} \times 100$, which is equivalent to the false alarm ratio, and $\frac{P_{ba}}{P_{ba}+P_{bb}} \times 100$, respectively (see Table 1).

[46] HSS values computed from the dynamically downscaled T_{max} are also positive over the most grid points except northwestern Alabama and a few grid points over southern Florida (Figure 14h). The dynamical downscaling method exhibits greater skill in Georgia as discussed in sections 4.2 and 4.3, resulting in higher HSS than that obtained from the statistical method. On the other hand, the

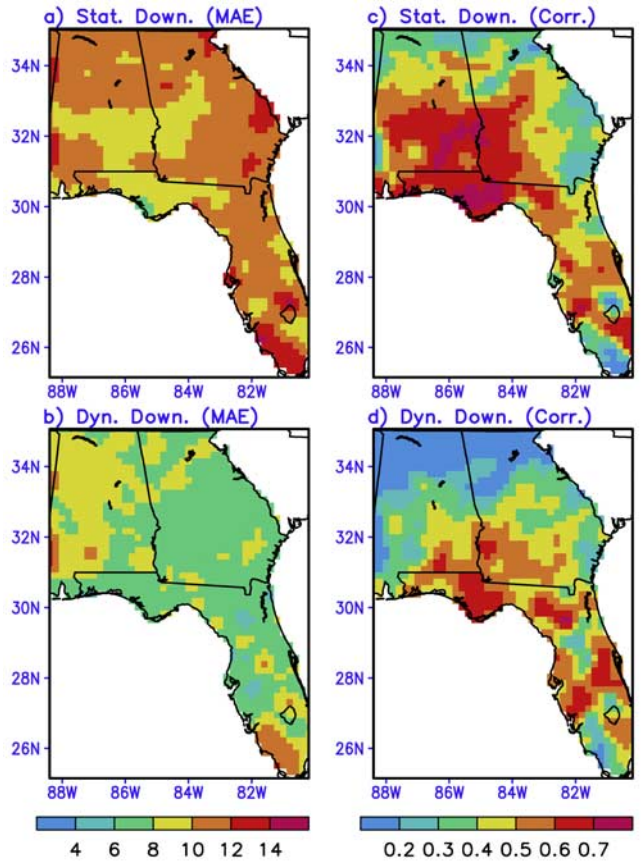

Figure 13. Distribution of mean absolute errors (left) and correlation coefficients (right) of seasonal variation in the frequency of extreme daily T_{max} events. Daily T_{max} exceeding 1 standard deviation above the climatological mean is defined as the extreme T_{max} event. (top) Result obtained from the statistical downscaling. (bottom) Dynamical downscaling. Color scale is denoted by color bar attached on the bottom of each column.

HSS of northwestern Alabama area for the dynamical method tends to be lower than that obtained from the statistical method. However, the overall spatial patterns of HSS clarifies that both downscaling methods are comparable, along with their reasonableness in simulating the seasonal warmness/coolness of local temperatures.

5. Concluding Remarks and Discussion

[47] Daily surface T_{max} simulated from the GSM ($\sim$1.875° lon.-lat., T63) have been downscaled to a spatial scale of 20 $\times$ 20 km for the southeastern region of the United States, covering Florida, Georgia, and Alabama. Regionalization is performed for spring and summer, for the period of 1994 to 2002 using dynamical and statistical methods.

[48] Dynamically downscaled surface temperatures are derived by running the NRSM, which is nested into the domain of the GSM. Results support that the NRSM model reasonably simulates fine-scale perturbations to the GSM simulations. Seasonal variations, anomalies, and changes in the number of extreme daily events for reginal surface T_{max} are successfully simulated by dynamical downscaling method.

[49] For statistical downscaling, a new method was developed in this study. The rationale for this approach is that clearer separation of prominent local climate signals (e.g., seasonal cycle, dominant intraseasonal or interannual oscillations) incorporated in the observations and the GSM over the training period can facilitate the identification of the statistical relationship associated with climate variability between two data sets, which eventually leads to better prediction of local climate scenario from the large-scale simulations. To this end, (1) CSEOF (Cyclostationary EOF) analysis is conducted on both observation and the GSM runs over the training period, followed by (2) regression between lower-mode PCs of observation and the GSM runs; as a result, the statistical relationship and corresponding regressed patterns are obtained. (3) CSEOF PC time series for prediction period is subsequently generated on the basis of the relationship identified from the first two steps. (4) The fine-scale data for the prediction period are constructed from the generated PC time series and the eigenfunctions obtained from training. (5) This procedure is repeated by withholding a particular year as a prediction period for the sake of cross validation.

[50] As summarized above, CSEOF is used instead of conventional eigentechniques such as regular EOF and SVD because the spatial patterns of each mode extracted from CSEOF represent the complete spatiotemporal evolution of the important climate signals (e.g., seasonal cycle, prominent intraseasonal oscillation, ENSO-related evolution, etc.) over a cyclic period [*Kim and Wu*, 1999]. The corresponding PC time series, which varies slowly with time, is usually easier to estimate for the future than the other conventional PC time series often exhibiting the noisy high-frequency fluctuations [*Lim and Kim*, 2006]. This downscaling approach therefore facilitates the generation of the subsequent PC time series for the prediction period, resulting in the better regionalized climate scenario from the large-scale simulations.

[51] Downscaled results are compared with observations and the GSM runs. Downscaled time series for T_{max} over local grid points faithfully reproduce the observed seasonal surface temperature variations and anomalies with significant reduction of warm/cold biases unveiled from the GSM. The majority of grid points for the simulation of local seasonal anomaly show correlations between 0.4 and 0.8. Regional differences in correlations and the categorical forecast show Florida and Georgia tend to be better downscaled than inland northwestern Alabama, where the GSM simulations were relatively poorer than coastal regions [*Cocke et al.*, 2007]. Downscaled anomalies exhibit temporal variations reliably but the general features reveal that better GSM simulations can improve downscaling results.

[52] The categorical forecast for the above/below climatological seasonal average shows that the percentage correct over most local grid points exceeds 60% and reaches up to 80%, which is remarkably greater than the predictability of random chance. The percentage incorrect, which is much lower than the percentage correct, and the corresponding HSS indicate that the simulation for the regional above/below climatological average is reasonably achieved by the downscaling approaches.

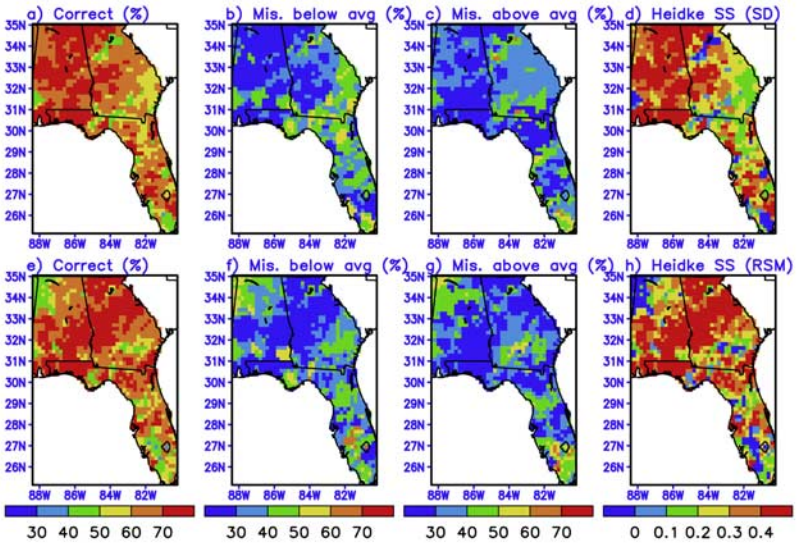

Figure 14. Categorical predictability in percentage (left three columns) and Heidke Skill Score (right column) for the downscaled seasonal T_{max} anomaly. Two classes from categorization are (1) above climatological T_{max} and (2) below climatological T_{max}. Result from the (top) statistical downscaling and (bottom) dynamical downscaling (the NRSM). First three columns from the left illustrate (1) the percentage of correct prediction (the sign of downscaled anomaly and observed anomaly is the same) (a, e), (2) $\frac{P_{ab}}{P_{aa}+P_{ab}} \times 100$ (see Table 1) (b, f), and (3) $\frac{P_{ba}}{P_{ba}+P_{bb}} \times 100$ (see Table 1) (c, g).

[53] In summary, on the basis of evaluations delineated above, we conclude that both downscaling methods are reliable in producing the regional climate scenario from coarsely resolved large-scale simulations. The reduction of the large-scale biases, the correlations with 0.4 to 0.8, and the percentage correct between 60 and 80% over most grid points can be considered acceptable as the skill of this local forecast is obtained in locations where the demonstrable skill is harder to achieve than other United States regions [*Saha et al.*, 2006]. Also, comparison between the two downscaling methods reveals that the methods exhibit comparable skill.

[54] Overall, it is not easy to conclude which method is preferable. We suggest that the statistical method for simulation of seasonal or monthly means and their anomalies is desirable because the method has skill comparable to that of the dynamical downscaling method without the computational expense, at least according to the skill measures used here. Many locations in the present study show better downscaled results using the statistical approach. On the other hand, reasons for selection of the dynamical approach is that dynamically downscaled fields for multiple variables are physically consistent. Therefore dynamically downscaled data may be more suitable for input for other application models (e.g., crop yield model) which critically depend on physical consistency. As for simulation of extreme events on a daily time interval, dynamical downscaling method tends to better simulate their frequency than statistical downscaling. Figure 12, which shows the simulation result for daily extreme event frequency, yields evidence of far greater overestimation or underestimation from the statistical downscaling. However, interannual variation of the frequency is better simulated by statistical downscaling as it shows greater correlation with observation.

[55] We have shown that the downscaling framework applied in this study is useful for providing near-surface regional seasonal temperature predictions which could be associated with urban impacts, agriculture and hydrology, and other vegetation characteristics. However, there is still room for the improvement in predictive skill. Not all grid points show high correlations with good skill scores. Northwestern Alabama has been poorly downscaled by dynamical downscaling whereas the statistical method fails to regionalize for the northeast and southeastern Georgia area with desirable skill score. Fixing these problems and the improvement in predictive skills over those areas will be the topic for further study. The present downscaling methods extended to other variables including precipitation will be also discussed in the next study.

[56] It should be mentioned that downscaling for a 9-year period using one ensemble member can be considered a limitation for drawing robust conclusions for the predictive skill of the two downscaling methods and their comparison. Although computationally expensive, using a large number

Table 1. Schematic Probability Table for Categorical Forecasts of Above/Below Climatological Average Event

	Downscaled Forecast		Marginal Probability Distribution for the Observation, Predictand, P
	Above Average	Below Average	
Observed Above	P_{aa}	P_{ba}	$P_a{}^P = P_{aa} + P_{ba}$
Observed Below	P_{ab}	P_{bb}	$P_b{}^P = P_{ab} + P_{bb}$
Marginal probability distribution for the forecast, F	$P_a{}^F = P_{aa} + P_{ab}$	$P_b{}^F = P_{ba} + P_{bb}$	1

of ensembles over a longer period are needed for a more critical evaluation. Our next study on downscaling of precipitation will be improved by applying multiple ensemble runs with a sufficiently longer period.

[57] **Acknowledgments.** FSU/COAPS receives its base support as a NOAA Applied Research Center, funded by the NOAA Climate Program Office. Additional support was provided by the USDA.

References

Barnston, A. G. (1992), Correspondence among the correlation, RMSE, and Heidke forecast verification measures: Refinement of the Heidke score, *Weather Forecast.*, *7*, 699–709.

Boé, J., L. Terray, F. Habets, and E. Martin (2006), A simple statistical-dynamical downscaling scheme based on weather types and conditional resampling, *J. Geophys. Res.*, *111*, D23106, doi:10.1029/2005JD006889.

Bonan, G. B., K. W. Oleson, M. Vertenstein, S. Levis, X. Zeng, Y. Dai, R. E. Dickinson, and Z.-L. Yang (2002), The land surface climatology of the Community Land Model coupled to the NCAR Community Climate Model, *J. Clim.*, *15*, 3123–3149.

Changnon, S. A. (1999), Impacts of 1997–98 El Niño-generated weather in the United States, *Bull. Am. Meteorol. Soc.*, *80*, 1819–1827.

Cocke, S. (1998), Case study of Erin using the FSU Nested Regional Spectral Model, *Mon. Weather Rev.*, *126*, 1337–1346.

Cocke, S., and T. E. LaRow (2000), Seasonal predictions using a regional spectral model embedded within a coupled ocean-atmosphere model, *Mon. Weather Rev.*, *128*, 689–708.

Cocke, S., T. E. LaRow, and D. W. Shin (2007), Seasonal rainfall prediction over the southeast U. S. using the FSU nested regional spectral model, *J. Geophys. Res.*, *112*, D04106, doi:10.1029/2006JD007535.

Conway, D., R. L. Wilby, and P. D. Jones (1996), Precipitation and air flow indices over the British Isles, *Clim. Res.*, *7*, 169–183.

Coulibaly, P., Y. B. Dibike, and F. Anctil (2005), Downscaling precipitation and temperature with temporal neural networks, *J. Hydrometeorol.*, *6*, 483–496.

Cressman, G. P. (1959), An operational objective analysis system, *Mon. Weather Rev.*, *87*, 367–374.

Díez, E., C. Primo, J. A. García-Moya, J. M. Gutiérrez, and B. Orfila (2005), Statistical and dynamical downscaling of precipitation over Spain from DEMETER seasonal forecasts, *Tellus, Ser. A*, *57*, 409–423.

Feddersen, H., and U. Andersen (2005), A method for statistical downscaling of seasonal ensemble predictions, *Tellus, Ser. A*, *57*, 398–408.

Fennessy, M. J., and J. Shukla (2000), Seasonal prediction over North America with a regional model nested in a global model, *J. Clim.*, *13*, 2605–2627.

Fuentes, U., and D. Heimann (2000), An improved statistical-dynamical downscaling scheme and its application to the Alpine precipitation climatology, *Theor. Appl. Climatol.*, *65*, 119–135.

Giorgi, F. (1990), Simulation of regional climate using a limited area model nested in a general-circulation model, *J. Clim.*, *3*, 941–963.

Giorgi, F., B. Hewitson, J. H. Christensen, M. Hulme, H. vonStorch, P. Whetton, R. Jones, L. O. Mearns, and C. Fu (2001), Regional climate information: Evaluation and projections, in *Climate Change 2001: The Scientific Basis*, chap. 10, pp. 583–638, Cambridge Univ. Press, Cambridge, UK.

Heidke, P. (1926), Berechnung des Erfolges und der Gute der Windstarke-vorhersagen im Sturmwarnungsdienst, *Geogr. Ann.*, *8*, 301–349.

Hewitson, B. C., and R. G. Crane (1996), Climate downscaling: Techniques and application, *Clim. Res.*, *7*, 85–95.

Hong, S.-Y., and A. Leetma (1999), An evaluation of the NCEP RSM for regional climate modeling, *J. Clim.*, *12*, 592–609.

Hoyer, J. M. (1987), The ECMWF spectral limited-area model, in *Workshop Proceedings on Techniques for Horizontal Discretization in Numerical Weather Prediction Models*, pp. 343–359, Eur. Cent. for Medium-Range Weather Forecasts, Reading, UK.

Huth, R. (2002), Statistical downscaling of daily temperature in central Europe, *J. Clim.*, *15*, 1731–1742.

Huth, R., and J. Kysely (2000), Constructing site-specific climate change scenarios on a monthly scale using statistical downscaling, *Theor. Appl. Climatol.*, *66*, 13–27.

Ji, Y., and A. D. Vernekar (1997), Simulation of the Asian summer monsoons of 1987 and 1988 with a regional model nested in a global GCM, *J. Clim.*, *10*, 1965–1979.

Jolliffe, I. T., and D. B. Stephenson (2003), *Forecast Verification: A Practitioner's Guide in Atmospheric Science*, 240 pp., John Wiley, Hoboken, N. J.

Juang, H. M., and M. Kanamitsu (1994), The NMC nested regional spectral model, *Mon. Weather Rev.*, *122*, 3–26.

Kim, K.-Y., and G. R. North (1997), EOFs of harmonizable cyclostationary processes, *J. Atmos. Sci.*, *54*, 2416–2427.

Kim, K.-Y., and Q. Wu (1999), A comparison study of EOF techniques: Analysis of nonstationary data with periodic statistics, *J. Clim.*, *12*, 185–199.

Lim, Y.-K., and K.-Y. Kim (2006), A new perspective on the climate prediction of Asian summer monsoon precipitation, *J. Clim.*, *19*, 4840–4853.

Marinucci, M. R., F. Giorgi, M. Beniston, M. Wild, P. Tschuck, and A. Bernasconi (1995), High resolution simulations of January and July climate over the western Alpine region with a nested regional modeling system, *Theor. Appl. Climatol.*, *51*, 119–138.

Misra, V., P. A. Dirmeyer, and B. P. Kirtman (2003), Dynamical downscaling of seasonal simulations over South America, *J. Clim.*, *16*, 103–117.

Murphy, J. (1999), An evaluation of statistical and dynamical techniques for downscaling local climate, *J. Clim.*, *12*, 2256–2284.

Nicolini, M., P. Salio, J. J. Katzfey, J. L. McGregor, and A. C. Saulo (2002), January and July regional climate simulation over South America, *J. Geophys. Res.*, *107*(D22), 4637, doi:10.1029/2001JD000736.

Ogura, H. (1971), Spectral representation of a periodic nonstationary random process, *IEEE Trans. Inf. Theory*, *17*, 143–149.

Oshima, N., H. Kato, and S. Kadokura (2002), An application of statistical downscaling to estimate surface air temperature in Japan, *J. Geophys. Res.*, *107*(D10), 4095, doi:10.1029/2001JD000762.

Pan, H.-L., and W. S. Wu (1994), Implementing a mass flux convection parameterization package for the NMC MRF model, in *10th Conference on Numerical Weather Prediction*, Preprints, pp. 96–98, Am. Meteorol. Soc., Portland, Ore.

Ramírez, M. C. V., N. J. Ferreira, and H. F. C. Velho (2006), Linear and nonlinear statistical downscaling for rainfall forecasting over southeastern Brazil, *Weather Forecast.*, *21*, 969–989.

Reusch, D. B., and R. B. Alley (2002), Automatic weather stations and artificial neural networks: Improving the instrumental record in west Antarctica, *Mon. Weather Rev.*, *130*, 3037–3053.

Robertson, A. W., S. Kirshner, and P. Smyth (2004), Downscaling of daily rainfall occurrence over northeast Brazil using a hidden Markov model, *J. Clim.*, *17*, 4407–4424.

Rotach, M. W., M. R. Marinucci, M. Wild, P. Tschuck, A. Ohmura, and M. Beniston (1997), Nested regional simulation of climate change over the Alps for the scenario of a doubled greenhouse forcing, *Theor. Appl. Climatol.*, *57*, 209–227.

Saha, S., et al. (2006), The NCEP climate forecast system, *J. Clim.*, *19*, 3483–3517.

Salathé, E. P. (2003), Comparison of various precipitation downscaling methods for the simulation of streamflow in a rainshadow river basin, *Int. J. Climatol.*, *23*, 887–901.

Salathé, E. P. (2005), Downscaling simulations of future global climate with application to hydrologic modeling, *Int. J. Climatol.*, *25*, 419–436.

Schmidli, J., C. M. Goodess, C. Frei, M. R. Haylock, Y. Hundecha, J. Ribalaygua, and T. Schmith (2007), Statistical and dynamical downscaling of precipitation: An evaluation and comparison of scenarios for the European Alps, *J. Geophys. Res.*, *112*, D04105, doi:10.1029/2005JD007026.

Schoof, J. T., and S. C. Pryor (2001), Downscaling temperature and precipitation: A comparison of regression-based methods and artificial neural networks, *Int. J. Climatol.*, *21*, 773–790.

Schubert, S., and A. Henderson-Sellers (1997), A statistical model to downscale local daily temperature extremes from synoptic-scale atmospheric circulation patterns in the Australian region, *Clim. Dyn.*, *13*, 223–234.

Shin, D. W., S. Cocke, T. E. LaRow, and J. J. O'Brien (2005), Seasonal surface air temperature and precipitation in the FSU climate model coupled to the CLM2, *J. Clim.*, *18*, 3217–3228.

Shin, D. W., J. G. Bellow, T. E. LaRow, S. Cocke, and J. J. O'Brien (2006), The role of an advanced land model in seasonal dynamical downscaling for crop model application, *J. Appl. Meteorol. Climatol.*, *45*, 686–701.

Sun, L., D. F. Moncunill, H. Li, A. D. Moura, F. D. A. D. S. Filho, and S. E. Zebiak (2006), An operational dynamical downscaling prediction system for nordeste Brazil and the 2002–04 real-time forecast evaluation, *J. Clim.*, *19*, 1990–2007.

Takayabu, Y. N., T. Iguchi, M. Kachi, A. Shibata, and H. Kanzawa (1999), Abrupt termination of the 1997–98 El Niño in response to a Madden-Julian oscillation, *Nature*, *402*, 279–282.

Trigo, R. M., and J. P. Palutikof (2001), Precipitation scenarios over Iberia: A comparison between direct GCM output and different downscaling techniques, *J. Clim.*, *14*, 4422–4446.

Widmann, M., C. S. Bretherton, and E. P. Salathe Jr. (2003), Statistical precipitation downscaling over the northwestern United States using numerically simulated precipitation as a predictor, *J. Clim.*, *16*, 799–816.

Wilby, R. L., and T. M. L. Wigley (1997), Downscaling general circulation model output: A review of methods and limitations, *Prog. Phys. Geogr.*, *21*, 530–548.

Wilby, R. L., T. M. L. Wigley, D. Conway, P. D. Jones, B. C. Hewitson, J. Main, and D. S. Wilks (1998), Statistical downscaling of general circulation model output: A comparison of methods, *Water Resour. Res.*, *34*, 2995–3008.

Wilks, D. S. (1999), Multisite downscaling of daily precipitation with a stochastic weather generator, *Clim. Res.*, *11*, 125–136.

Wood, A. W., E. P. Maurer, A. Kumar, and D. P. Lettenmaier (2002), Long-range experimental hydrologic forecasting for the eastern United States, *J. Geophys. Res.*, *107*(D20), 4429, doi:10.1029/2001JD000659.

Xu, C.-Y. (1999), From GCMs to river flow: A review of downscaling methods and hydrologic modelling approaches, *Prog. Phys. Geogr.*, *23*, 229–249.

Zhu, J., and X.-Z. Liang (2007), Regional climate model simulations of U.S. precipitation and surface air temperature during 1982–2002: Interannual variation, *J. Clim.*, *20*, 218–232.

E. P. Chassignet, S. Cocke, T. E. LaRow, Y.-K. Lim, J. J. O'Brien, and D. W. Shin, Center for Ocean-Atmospheric Prediction Studies (COAPS), Florida State University, Tallahassee, FL 32306-2840, USA. (lim@coaps.fsu.edu)

J. T. Schoof, Department of Geography and Environmental Resources, Southern Illinois University, Carbondale, IL 62901, USA.